# **Neuron**

## **Clonally Related Forebrain Interneurons Disperse Broadly across Both Functional Areas and Structural Boundaries**

## **Highlights**

- Clonal dispersion of GABAergic neurons occurs across large areas of the forebrain
- Lineage does not determine the allocation of interneurons to particular regions
- Interneurons emerge from asymmetric progenitor and symmetric neurogenic divisions

## **Authors**

Christian Mayer, Xavier H. Jaglin, Lucy V. Cobbs, ..., Constance L. Cepko, Simon Hippenmeyer, Gord Fishell

## Correspondence

fisheg01@nyumc.org

## In Brief

Most GABAergic interneurons in the mouse are generated in the ventral embryonic forebrain and reach their final destination (e.g., in the cortex) through tangential migration. Using a replicationdefective retroviral library containing a highly diverse set of DNA barcodes, Mayer et al. show that clonally related interneurons disperse across functional and anatomical boundaries within the forebrain.





## **Clonally Related Forebrain Interneurons Disperse Broadly across Both Functional Areas** and Structural Boundaries

Christian Mayer, Xavier H. Jaglin, Lucy V. Cobbs, Rachel C. Bandler, Carmen Streicher, Constance L. Cepko, Simon Hippenmeyer,<sup>2</sup> and Gord Fishell<sup>1,\*</sup>

<sup>1</sup>NYU Neuroscience Institute, NYU Langone Medical Center, New York, NY 10016, USA

http://dx.doi.org/10.1016/j.neuron.2015.07.011

#### **SUMMARY**

The medial ganglionic eminence (MGE) gives rise to the majority of mouse forebrain interneurons. Here, we examine the lineage relationship among MGEderived interneurons using a replication-defective retroviral library containing a highly diverse set of DNA barcodes. Recovering the barcodes from the mature progeny of infected progenitor cells enabled us to unambiguously determine their respective lineal relationship. We found that clonal dispersion occurs across large areas of the brain and is not restricted by anatomical divisions. As such, sibling interneurons can populate the cortex, hippocampus striatum, and globus pallidus. The majority of interneurons appeared to be generated from asymmetric divisions of MGE progenitor cells, followed by symmetric divisions within the subventricular zone. Altogether, our findings uncover that lineage relationships do not appear to determine interneuron allocation to particular regions. As such, it is likely that clonally related interneurons have considerable flexibility as to the particular forebrain circuits to which they can contribute.

## INTRODUCTION

Understanding the principles by which brain circuits are constructed is a fundamental goal in developmental neuroscience. The assembly of complex brain circuitry begins with the generation of prescribed cell types from what are thought to be stereotyped lineages. While neuronal lineages have been well documented in invertebrates (Kohwi and Doe, 2013), the relationships between progenitors and their progeny are less clear in vertebrates. Over 25 years ago, a retroviral lineage approach was developed that provided the means to identify lineages within different areas of the central nervous system (CNS) (Golden et al., 1995; Walsh and Cepko, 1992). These efforts provided the first indications that lineages within the cortex do not necessarily result from a precisely orchestrated transposition of cells from the proliferative zone to post-mitotic

Following these original studies, a number of methods have been developed that allow for the directed labeling and tracking of progenitors from discrete proliferative zones (Ciceri et al., 2013; García-Moreno et al., 2014; Vasistha et al., 2014; Yu et al., 2009; Zong et al., 2005). In the cortex, the use of these methods indicates that pyramidal cell migration is more radially coherent than was previously thought. While some degree of dispersion occurs, the majority of clones populate columns and even participate functionally in common circuits as predicted by Rakic's "protomap" hypothesis (Rakic, 1988).

A similar understanding of the subpallial-derived interneuron lineages has yet to be achieved. Work from several laboratories, including our own, has demonstrated that inhibitory interneuron populations are entirely derived from the subpallium (reviewed in Fishell and Rudy, 2011; Figure 1A), most prominently from the medial and caudal ganglionic eminences (medial ganglionic eminence [MGE] and CGE, respectively). In mice, the MGE produces 70% of all cortical interneurons and the entirety of both the parvalbumin and somatostatin populations, not only within the cortex (Miyoshi et al., 2007) but also in the associated hippocampus (Tricoire et al., 2011), as well as in subpallial structures, such as the striatum (Marin et al., 2000) and amygdala nuclei (Nery et al., 2002).

Two recent studies have attempted to connect the lineage relationship of MGE-derived interneurons to their cell type and position (Brown et al., 2011; Ciceri et al., 2013). These groups used mouse genetics to specifically label interneuron progenitor cells in the MGE with fluorescently tagged retroviruses. Their results suggested that interneurons arising from a common progenitor preferentially form clusters within either cortical layers and/or columns. An inherent limitation of this approach is that dispersed interneurons labeled with the same fluorophore were assumed ab initio to be derived from independent clones.

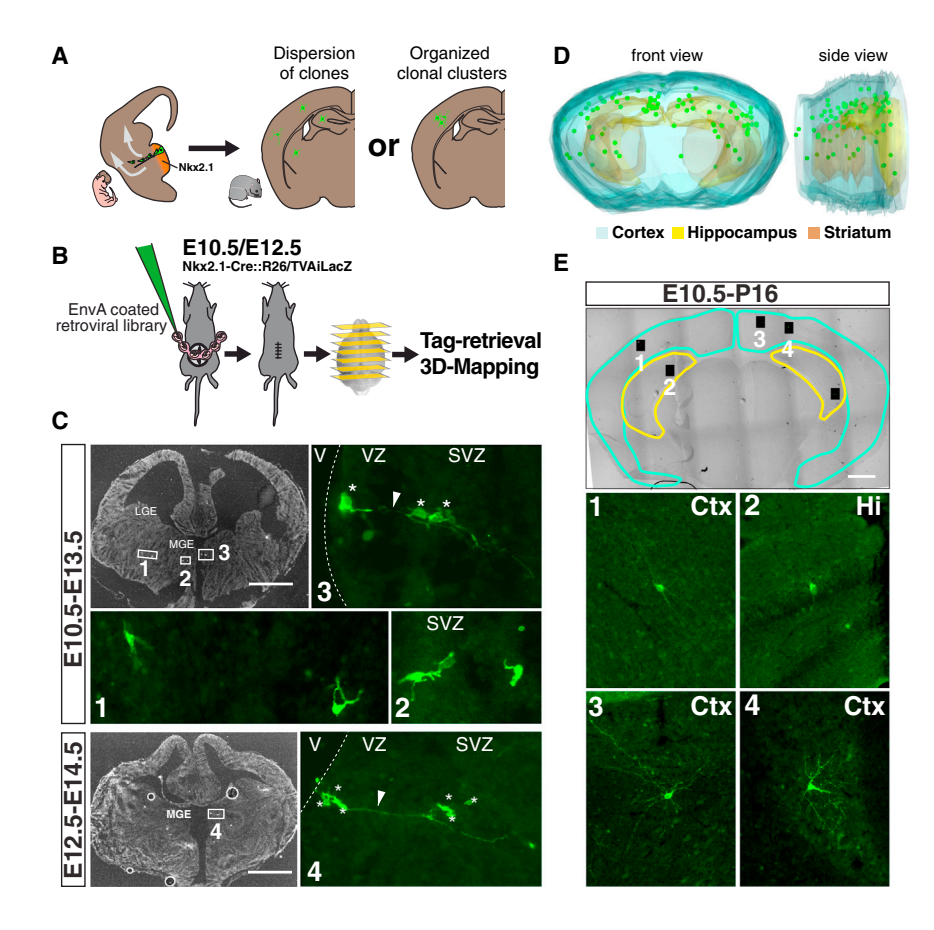
To overcome this drawback, we have reinvestigated this question using a barcoded GFP-expressing retroviral library (Golden et al., 1995), restricted in its infection to progenitor cells of the MGE that express the avian virus receptor, TVA, as dictated by a Cre-dependent TVA reporter allele (Seidler et al., 2008).



<sup>&</sup>lt;sup>2</sup>Institute of Science and Technology Austria, 3400 Klosterneuburg, Austria

<sup>&</sup>lt;sup>3</sup>Departments of Genetics and Ophthalmology and HHMI, Harvard Medical School, Boston, MA 02115, USA

<sup>\*</sup>Correspondence: fisheg01@nyumc.org



To our considerable surprise, while a minority of clones were found to be densely clustered, the majority of MGE clones dispersed over large areas, both within and across telencephalic structures. Complementing these efforts, we analyzed the acute dispersion of clones using both retroviral and MADM (mosaic analysis with double markers) approaches in the context of shortsurvival periods. These experiments indicated that most MGE lineages originate from radial glia progenitors in the MGE ventricular zone (VZ) and can be locally amplified in the subventricular zone (SVZ). We conclude that while sibling interneurons may occasionally form coherent clusters, the final positions of clonally related interneurons are generally not constrained by lineal relationships.

## **RESULTS**

## **Selective Targeting of Interneuron Progenitor Cells** within the MGE with a Barcoded Retroviral Library

To identify the cortical interneuron populations produced by individual MGE progenitor cells, we used ultrasound-backscatter microscopy (UBM)-guided microinjection to inject a retroviral library into the lateral ventricles of transgenic E10.5-E12.5 embryos, the beginning of the peak phase of interneuron neurogenesis in this region (Miyoshi et al., 2007; Figures 1A and 1B). The viral library encodes GFP and contains approximately 105 random 24-bp oligonucleotide tags (barcodes). To retrieve barcodes, infected cells can be identified by GFP and collected from brain sections by laser capture microdissecion (LCM). Due to the

Figure 1. Targeted Infection of MGE Progenitor Cells with a Retroviral Library

(A) A diagram summarizing the experimental design of this study. Orange depicts the area of Nkx2.1-Cre expression.

(B) The experimental strategy.

(C) Overview images (black-and-white) and highmagnification images (green) of sections of embryonic mouse brains 2 to 3 days after injection of a retroviral library at E10.5 or E12.5. Radial clusters of cells expressing GFP (green, asterisks) were found in the VZ and SVZ of the MGE, but not the CGE, LGE, or cortex. Several cells with short processes (white asterisks) are arrayed along a radial process (white arrows).

(D) 3D reconstruction illustrating the distribution of GFP-expressing neurons with a barcode in the forebrain of a P16 mouse that was infected with a retroviral library at E10.5.

(E) Representative high-magnification images and their location within a 25-µm coronal brain section in the cortex (cyan tracing) and hippocampus (yellow tracing). Ctx, cortex; Hi, hippocampus. Scale bars, 500 um.

See also Figure S1.

high complexity of the library, and the relatively low number of clones, cells sharing the same barcode are almost certainly siblings (Golden et al., 1995; Fuentealba et al., 2015). The retroviral library used here was pseudotyped with

the ASLV-A envelope glycoprotein (EnvA), which restricts infection to cells expressing the cognate avian virus receptor for this glycoprotein, TVA (Bates et al., 1993). We conditionally expressed TVA in mitotic cells of the MGE by crossing an MGE-specific transgenic Cre driver line (Nkx2.1-Cre: Xu et al., 2008) with R26-TVAiLacZ (Seidler et al., 2008) mice. As predicted, 2 to 3 days after the injection of the retroviral library, isolated radially oriented clusters of GFP-expressing cells were observed in the VZ of the MGE, but not in other progenitor zones of the subpallium or neocortex (Figure 1C). No GFP labeling was observed in the brains of animals that did not encode TVA (Nkx2.1+/+;R26LSL-TVAiLacZ/+ littermates; data not shown). To study the distribution and fate of cells derived from Nkx2.1-Cre expressing cells, Nkx2.1<sup>Cre/+</sup>;R26<sup>LSL-TVAiLacZ/+</sup> embryos were injected with the retroviral library at E10.5 and sacrificed at P16, by which time migration of interneurons is largely complete (Corbin et al., 2001). At P16, GFP-positive neurons were found in a variety of regions throughout the telencephalon (Figures 1D, 1E, and S1), including the neocortex, striatum, olfactory bulb, hippocampus, globus pallidus, hypothalamus, and septum, as well as in oligodendrocytes of subcortical structures, consistent with the findings from Nkx2.1 genetic fate-mapping studies (Kessaris et al., 2006; Xu et al., 2008). The barcodes from 47-90 (61  $\pm$  14; n = 3; Figure 2A) GFP-positive neurons were sequenced per brain. 44% (±16%; n = 3) of the analyzed neurons carried a unique barcode, indicating that they were either single-cell clones or that we failed to sample a sibling cell.

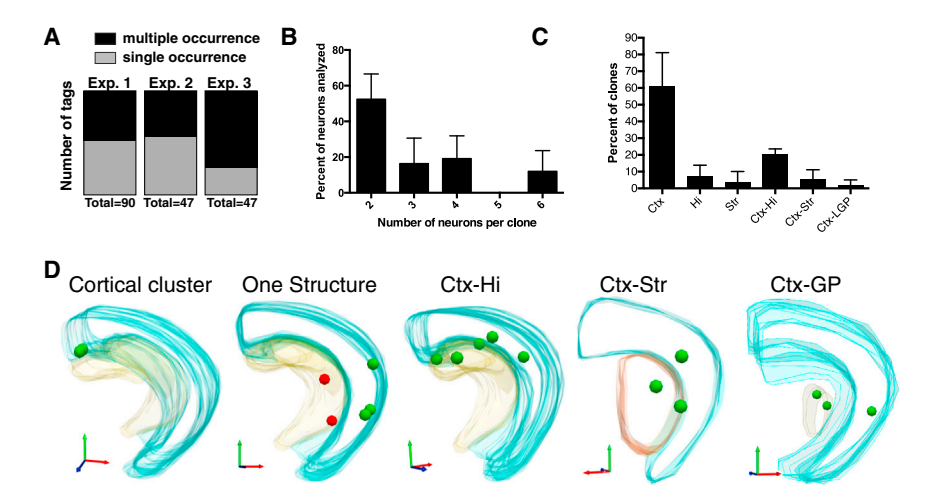


Figure 2. Dispersion of Interneuron Clones across Forebrain Structures

- (A) Quantification of single-cell and multi-cell clones identified by barcode analysis.
- (B) A histogram illustrating the probability in percent that barcoded neurons contribute to a clone of a particular size.
- (C) Categorization of clones according to their spread. Ctx, cortex; Hi, hippocampus; Str, striatum; GP, globus pallidus; n = 3 brains.
- (D) 3D reconstructions of five clones (green or red dots) illustrating different modes of dispersion. Error bars represent SD.

56% ( $\pm$ 16%, n = 3; Figure 2A) of the barcodes, however, were members of multi-cell clones, ranging in size from two sibling cells (by far the majority;  $52\% \pm 14\%$ ; n = 3), up to six sibling cells (12%  $\pm$  12%; n = 3; Figure 2B).

## **Dispersion of Clonally Related Interneurons across Brain Structures**

To systematically examine the distribution of clonally related interneurons (i.e., neurons with identical barcodes), the Cartesian coordinates of neurons with recovered barcodes were determined for the cortex, hippocampus, striatum, and globus pallidus. More than 50% of GFP-labeled multi-cellular clones were located in the cortex (61% ± 20% cortex; Figure S2;  $7\% \pm 6\%$  hippocampus,  $3\% \pm 6\%$  striatum; n = 3; Figure 2C). Strikingly, a number of clonally related neurons were not restricted to only one structure; rather, they were distributed across anatomically and functionally distinct regions of the forebrain. For example, some clones populated the cortex and hippocampus (20%  $\pm$  3%, n = 3), the cortex and striatum  $(6\% \pm 6\%, n = 3)$  or the cortex and globus pallidus  $(2\% \pm 3\%, n = 3)$ n = 3; Figure 2C). By contrast, clones of the telencephalon did not share barcodes with clones in the hypothalamus or contralateral hemisphere, indicating that MGE-derived neurons are restricted to the ipsilateral telencephalon (data not shown). Moreover, identical barcodes were very rarely recovered within different retrovirally infected brains, indicating that the complexity of the library is sufficient to unambiguously resolve lineage relationships. In an attempt to assess the subtype identity of infected neurons, we did immunocytochemical analysis in a subset of clones analyzed. In accordance with previous findings (Brown et al., 2011; Ciceri et al., 2013), the existence of clones consisting of entirely parvalbumin-positive clones, as well as of mixed parvalbumin-positive and parvalbumin-negative clones (presumably the majority of the later were somatostatin neurons [Miyoshi et al., 2007]), were observed (Figure S3).

## **Dispersion of Clonally Related Interneurons within Brain Structures**

If the lineage relationship contributed to the functional organization of inhibitory interneurons within the mammalian neocortex, one would expect that interneuron clones would reside in close proximity and within similar functional units of the cortex (Yu et al., 2009). To test whether clonally related interneurons settle within focal areas, we calculated the Euclidean distances between pairs of sibling cells within brain structures (Figure 3A) and analyzed their distribution (Figure 3B). Pairs of clonally related neurons were on average almost 2,000 µm apart  $(1.947 \pm 1.274 \mu m; n = 49 pairs of neurons)$ , and only 8% of the pairs were located within 500 µm of each other. The average distance between clonally related cells was 1,885  $\mu m$ ( $\pm$  1,132  $\mu$ m; n = 20 clones) in the cortex, 1,517  $\mu$ m ( $\pm$  554  $\mu$ m; n = 5 clones) in the hippocampus, and 982  $\mu$ m (± 495  $\mu$ m; n = 3 clones; Figure 3C) in the striatum. This analysis shows that sibling interneurons reside in a volume that exceeds functional cortical units, such as whisker barrels of the somatosensory cortex (400 µm; Bruno et al., 2003; Mountcastle, 2003).

Next, we asked whether lineal relationship predicts the position of sibling cells within the cortex, hippocampus, or striatum. We reasoned that if this was the case, then clonally related neurons should preferentially be clustered compared to members of unrelated interneuron lineages. To test this, we examined the lineage relationship of localized clusters. We first grouped GFP-labeled neurons, regardless of their lineage by their proximity and displayed the results in dendrograms (Figures 3D and S4). We then labeled the neurons according to their lineage relationship (i.e., barcode identity). Fourteen out of 27 clones did not form isolated clusters. The isolated clonal clusters that we did observe (Figures 3D and 3E; #2, #7, #8, #11, #16, #21, #22, #24, #25, #26, #28, and #30) were mainly two-cell clusters, of which five (clone #2, #11, #25, #26, and #31) had additional sister cells outside the isolated cluster (splitting). The average distance between isolated clonally related cells (splitting cells not included) was 869  $\mu$ m (± 593  $\mu$ m; n = 13 cluster; Figure 3E). Next, we included single-cell barcodes (i.e., neurons with unique barcodes) into the analysis to increase the pool of interneurons and calculated the nearest-neighbor distance (NND) and the average distance (AD) between pairs of neurons. As expected, the NND of unrelated neurons was significantly smaller (560 ± 337 μm; n = 185 interneuron pairs) than that of sibling neurons  $(1,550 \pm 965 \mu m; n = 84; p < 0.0001; Figure 2E)$ . Strikingly, there

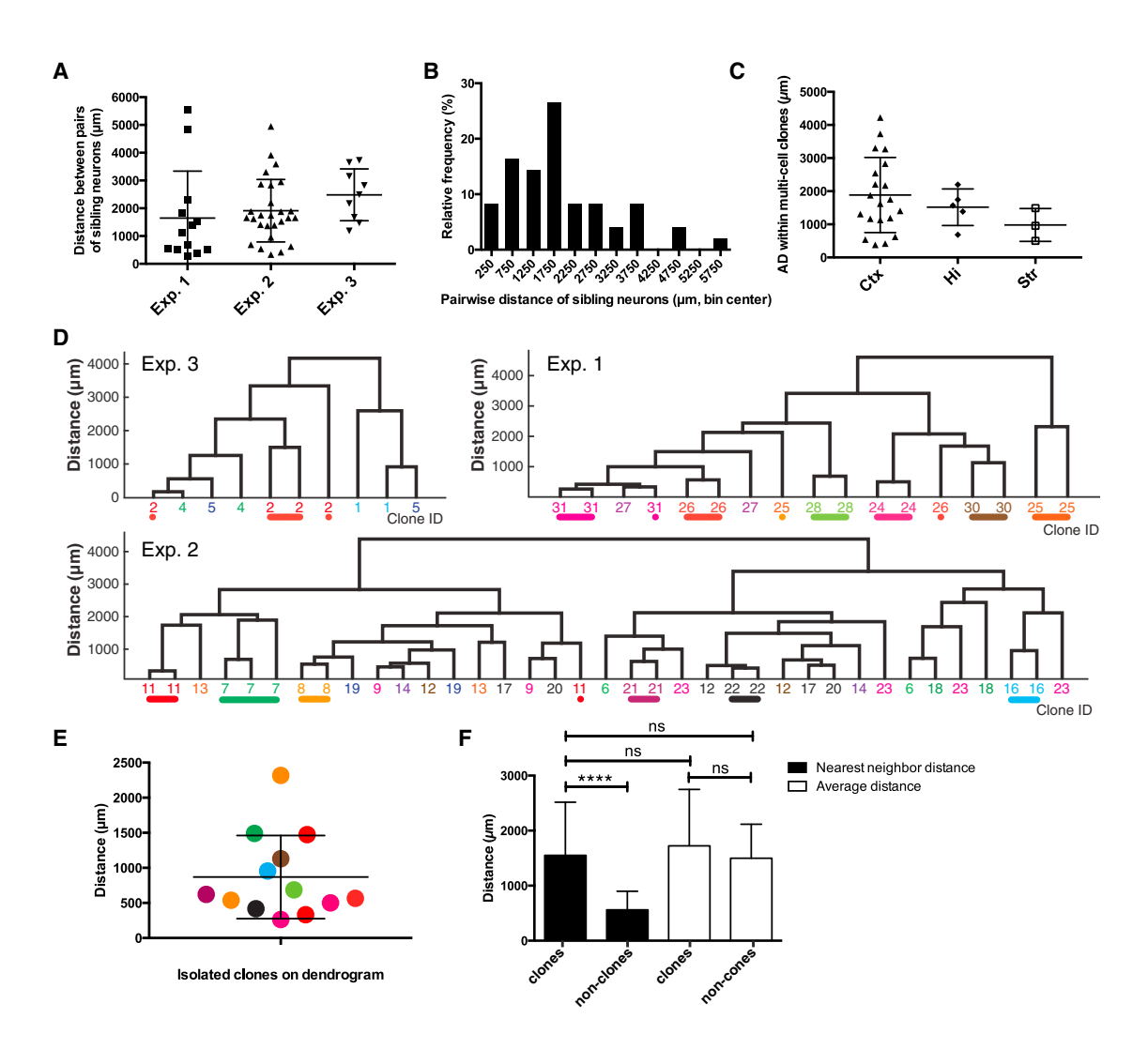


Figure 3. Dispersion of Clonally Related Interneurons within Brain Structures

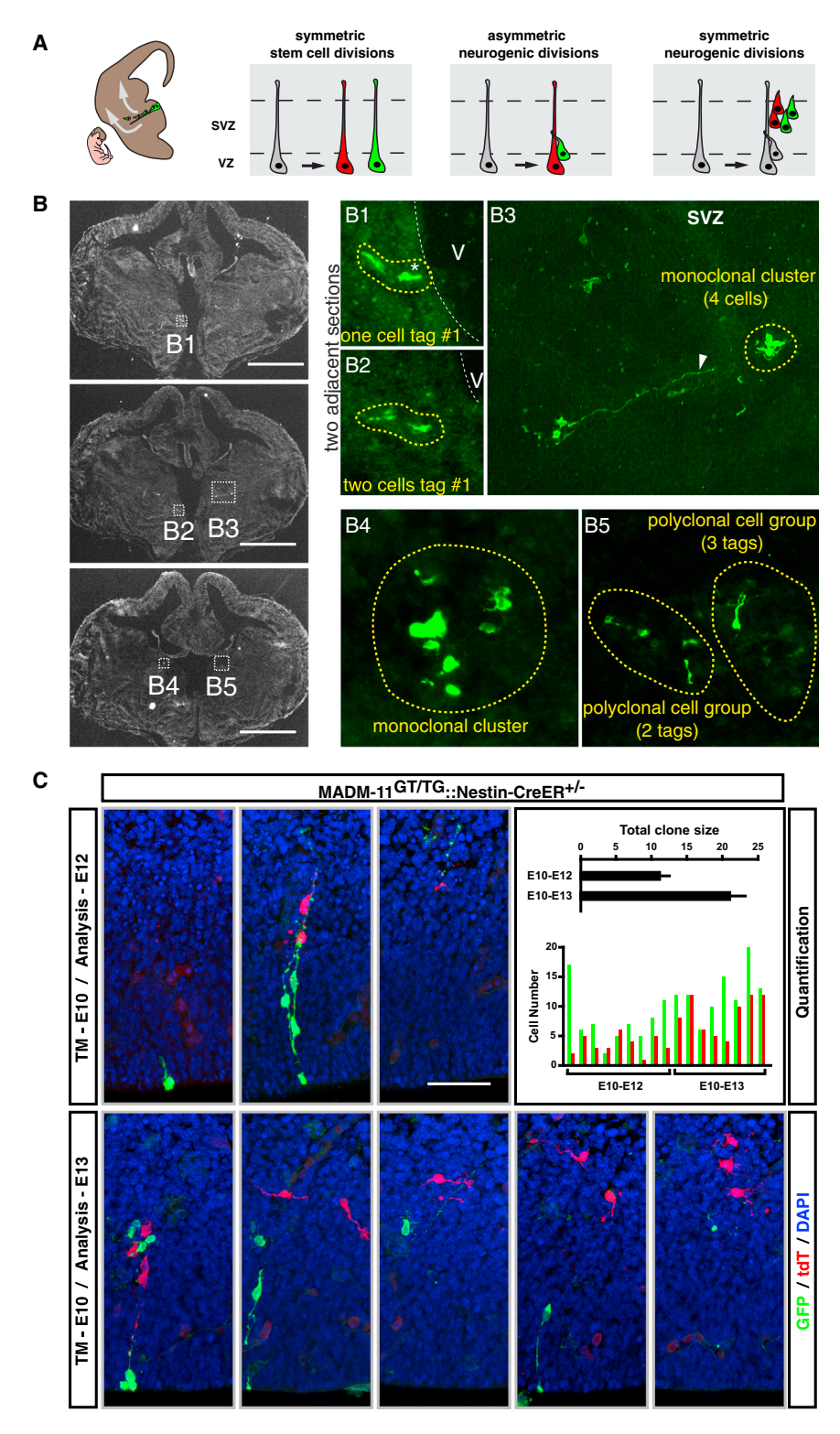
- (A) Pairwise distances of all multi-cell clones that were restricted to one brain structure are shown for three experiments (three analyzed brains).
- (B) A histogram of pairwise distances for pooled data of three experiments. Bin size, 500  $\mu m$ .
- (C) Average distances between neurons within clones in the cortex, hippocampus, and striatum.
- (D) Dendrograms showing hierarchical relationships between clones of one brain structure grouped according to their Euclidian distances and labeled according to their lineal relationship. Numbers and colors indicate the lineal relationship between two or more cells based on barcode sequencing. Colored lines below numbers mark isolated clonal clusters; colored dots mark split sibling neurons of the latter.
- (E) Quantification of the distance between isolated clonal clusters.
- (F) Nearest-neighbor distance and average distance of multi-cell clones of one structure (clones) and all labeled neurons with a barcode (non-clones). Error bars represent SD.

See also Figures S2 and S4.

was no significant difference in the AD between pairs of sibling neurons and pairs of unrelated neurons (1,498  $\pm$  617.5  $\mu$ m; n = 17; versus  $1,723 \pm 1,027 \mu m$ ; n = 28; p = 0.8; Figure 3F). Furthermore, no significant difference was detected between the NND and the AD of clones (Figure 3F), indicating that splitting of clonal clusters into two or more clusters is not a common mode of organization. Grouping members of clones according to their proximity into dendrograms resulted in only five isolated clusters when single-cell barcodes were included in the analysis (Figure S4).

### **Organization of Interneuron Progenitor Cells in the MGE**

In interpreting the significance of our findings, it is essential to determine the mode of cell division that progenitors undergo after retroviral labeling. We examined the lineages of newly postmitotic interneurons within selected samples of GFP-positive cells in the VZ and SVZ, 2 to 3 days post-infection with the retroviral library. Because individual cells within dense clusters of GFPpositive cells could not be separated using LCM, cells were captured as groups. PCR fragments harboring the barcodes were subcloned into plasmids and transformed into competent



bacterial cells. Sequencing the barcodes of multiple bacterial colonies allowed an estimation of the number of barcodes per cluster and the identification of their sequence. Figure 4B shows representative images illustrating the clonal organization within the

Figure 4. Spatially Organized Clonal Units in the MGE

(A) A diagram illustrating the different kinds of cell divisions that have previously been described in the MGE of embryonic mice (Brown et al., 2011). (B) High-magnification images of groups of neurons (green) and their exact location depicted within low-magnification overview images of coronal brain sections (black-and-white images). Rectangles indicate the location of high-magnification images; yellow circles and labels indicate the clonal relation between groups of neurons (i.e., monoclonal clusters or polyclonal cell groups). (C) Representative examples of E10-E12 and E10-E13 MADM clones in the VZ/SVZ of the MGE. The total clone size was  $11.1 \pm 1{,}389 (n = 9)$  for E10-E12 and 21  $\pm$  2,188 (n = 8) for E10-E13, respectively. The majority of G2-X MADM clones (15/17) display unequal lineage trees with respect to the absolute number of labeled neurons in the two (red and green) sublineages. Scale bars, 500 μm (B), 50 μm (C). Error bars represent SEM.

MGE. Similar to published observations

See also Figure S5.

(Brown et al., 2011), we found evidence for radially aligned clones, with one cell touching the ventricular surface and additional cells being symmetrically aligned in close vicinity (Figures 4B1 and 4B2; n = 6), likely demonstrating asymmetrical progenitor divisions (Figure 4A; Brown et al., 2011; Noctor et al., 2001). We also found monoclonal clusters in the SVZ that were often attached to radial glia fibers (Figures 4B3 and 4B4; n = 9), suggesting that symmetrical terminal divisions occur in the SVZ (Brown et al., 2011; Noctor et al., 2004). With increasing distance from the ventricular surface, clonal boundaries became indistinct and were impossible to predict. Patches of laser-captured tissue from these samples contained multiple cells with multiple barcodes (Figure 4B5; n = 9). At this stage, cells were not attached to radial glia fibers, likely indicating the mixing of distinct lineages as a result of the migration of neuronal precursor cells. We did not find evidence for shared barcodes between radial glia, and we also did not observe symmetric radial glial divisions. Taken together, our results suggest that clonal dispersion throughout the forebrain arises

from asymmetrical progenitor divisions, accompanied by symmetrical terminal divisions within the SVZ.

To independently assess the mode of divisions within MGE progenitors at this developmental stage, we analyzed clones at

different time points using the MADM method (Zong et al., 2005), which provides single-cell resolution of progenitor division pattern. A key MADM feature is the ability to induce clones of distinctly labeled neurons originating from a single dividing progenitor cell in a temporally defined fashion using tamoxifen (TM)-inducible CreER driver lines (Bonaguidi et al., 2011; Hippenmeyer et al., 2010; Zong et al., 2005; Figure S5). To achieve selective labeling of interneuron progenitors and their progeny, we used MADM-11 in combination with Nestin-CreERT2 (Hippenmeyer et al., 2010). A single TM dose was administered to timed pregnant Nestin-CreERT2/MADM-11 dams at E10 via intraperitoneal injection. Embryonic brains were recovered 2 or 3 days post-TM injection, processed for serial cryosectioning and immunostained to visualize all MADM-labeled cells in the VZ/SVZ of the MGE. The MADM-labeling efficiency of MGE progenitors was very low (less than one clone per brain on average) and in the absence of TM treatment, we found no labeled cells. MADM clones in the MGE displayed radially arrayed clusters of cells in the VZ (Figure 4C) and clumpy clusters of cells in the SVZ, both found in close proximity to a radial glia process. Consistent with our retroviral findings, individual clusters contained either a combination of green and red fluorescent neurons (G-X clone; Figure 4C) or yellow fluorescent neurons only (G2-Z or G1 events; data not shown). The majority of MADM clones (15/17) displayed labeling consistent with asymmetric neurogenic divisions, as indicated by the presence of an unequal amount of red and green cells within a cluster. In addition, a much smaller number (2/17) of MGE progenitors produced symmetric lineage trees within the 2- to 3-day developmental time window (Figure 4C, upper right). Within the distinctly labeled MADM subclones, we frequently observed clusters of labeled cells in the SVZ similar to the above clones labeled with retrovirus. Upon exiting the MGE SVZ, MADM-labeled cells dispersed widely and migrated toward the dorsal telecephalon. This corroborates our interpretation that MGE progenitors undergoing active neurogenesis produce a widely dispersed progeny that contributes to a variety of telencephalic structures in a seemingly unconstrained manner. Our data suggest that (1) retrovirally labeled clones of future neocortical and hippocampal interneurons in the MGE are initially organized into radial arrays, similar to clones of excitatory neurons (Brown et al., 2011; Rakic, 1988) and (2) intermediate progenitors in the MGE SVZ further amplify the number of post-mitotic interneurons through symmetric neurogenic divisions (Figure 4A; Noctor et al., 2004).

## Dispersion of Clonally Related Cells after Uncovering Transcriptionally Silenced Viral Vectors

The number of cells per clone was surprisingly large in short-term analysis (Figure 4C) compared with clones examined after migration (Figure 2B). Previous lineage studies (Cepko et al., 2000; Halliday and Cepko, 1992; McCarthy et al., 2001) in the forebrain have noted transcriptional silencing of retroviral vectors. As we identified barcoded neurons based on their expression of GFP, transcriptional silencing of GFP by P16 could explain the observed discrepancy in clone size. To recover putative barcodes regardless of silencing, we collected large pieces of tissue from brain sections of P16 mice that were infected with the retroviral library at E10.5. From the same sections, in which

all GFP-expressing neurons had previously been individually collected via LCM (exp. 3 in Figures 2A and 3A), we processed 228 pieces of cortical, hippocampal, and striatal tissue. These were collected from individual 25 µm coronal brain sections to maintain the spatial resolution of neurons with silenced barcodes. Barcodes were PCR amplified, ligated into plasmids, and transformed into bacterial cells. Sequencing of a large number of plasmids (1,026, of which the vast majority was repetition of identical barcodes due to oversampling of bacterial colonies), each isolated from a single bacterial colony, indicated that every coronal brain section contained on average 1.8 ± 1.4 silenced barcodes per structure (n = 3 structures). The results were added to the existing dataset of identified barcodes, increasing the number of recovered barcodes from 47 to 406 (Figures 2A and 5C). These data indicate that a large amount of retroviral silencing occurred by P16. Recovering silenced barcodes reduced the percentage of single-cell clones from  $44\% \pm 16\%$ (n = 3 brains) to 32% (n = 1 hemisphere; Figure 5B), suggesting that many singletons in the previous experiments had siblings with silenced vectors. When clones were plotted according to their location along the anterior-posterior axis (Figure 5C), a large spread of clonally related interneurons was evident. Despite adding a few large clones (including one 13-cell and one 15-cell clone), the number of neurons per clone did not markedly change (Figures 2B and 5D). In addition, the relative distribution of clones within and across different structures of the forebrain was similar when silenced clones were added to the analysis (Figure 5E). Notably, the AD between pairs of related cells was similar to unrelated cells. Hence, these results provide further support for the widespread dispersion of MGE-derived clones within the ipsilateral telencephalon.

## **DISCUSSION**

Our analysis provides a description of the relationship between MGE-derived interneuron lineages and their global distribution within the telencephalon. Examination of the final position of MGE-derived interneuron clones within the brain revealed a dramatic dispersion of sister cells both within and across structural boundaries within the telencephalon. By contrast, clones were not seen to cross the segmental boundary of the diencephalon and telencephalon or the midline between the two cerebral hemispheres. While it remains possible that some clones occupy small functional units in the forebrain, they would be in the minority, as most clones observed here were widely distributed.

A fundamental parameter needed to interpret these results was the mode of division that the infected progenitor cells underwent subsequent to retroviral integration. If the clones resulted from symmetric self-renewing stem cell (i.e., non-neurogenic) divisions, it would perhaps not be surprising that a high degree of dispersion was observed. By contrast, if the clones were produced from asymmetric neurogenic divisions, it would imply an unexpected ability for lineage-related clones to be allocated to distinct structures. We utilized two independent approaches to ascertain the mode of cell division. First, we examined the distribution of infected cells containing retroviral barcodes 1 to 3 days post-infection, and second, we utilized MADM (Zong et al.,

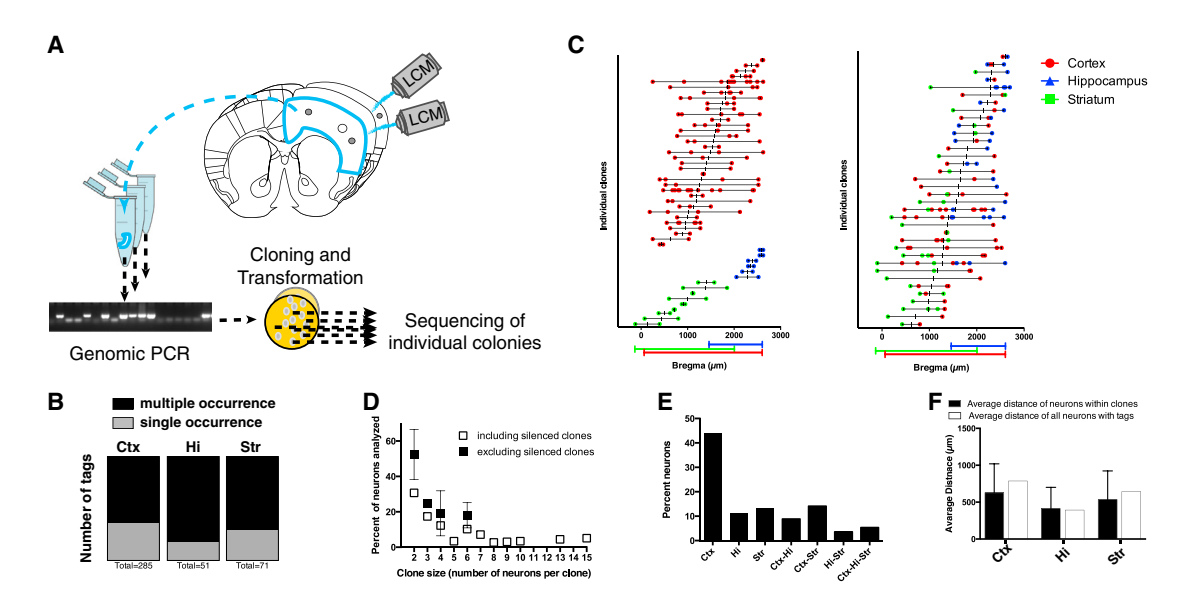


Figure 5. Distribution of Transcriptionally Silenced Viral Vectors

(A) A schematic illustrating the strategy to recover silenced barcodes. Note: the spatial resolution of silenced barcodes is maintained only by anatomical structure and within the anterior-posterior axis.

(B) Quantification of single-cell and multi-cell clones identified by barcode analysis.

(C) The location of both GFP-positive- and GFP-negative-infected neurons is plotted on the x axis relative to Bregma. Dots connected with a horizontal line represent the location of sibling neurons. Left: sibling cells that were dispersed either within the cortex (red), hippocampus (blue), or striatum (green). Right: barcodes represent sibling cells that were spread across structural boundaries.

(D and E) Relative clonal size (D) and spread both within and across brain structures (E).

(F) The AD of multi-cell clones and single-cell clones in different brain structures. Error bars represent SD.

2005), in which recombination in progenitor cells leads to the production of green or red fluorescent protein in the two daughter cells. The results from both analyses supported a model in which the majority of MGE-derived interneurons were generated by neurogenic amplification divisions.

In comparing the short-term and long-term analysis of clones, we observed that the clone size differed substantially. We speculate that the relatively small clone size observed at P16 is attributable to a combination of significant cell death occurring during interneuron maturation (Southwell et al., 2012), a degree of failure in the capture of sibling cells, and as a result of progressive increases in retroviral silencing with age. In contrast to studies relying purely on the expression of retroviral marker genes, the genomic barcodes allowed us to estimate the amount of silencing and even to include barcodes obtained from silenced vectors into our analysis (although doing so came at the price of reducing the spatial resolution compared to neurons captured based on GFP-expression, because the position of silenced clones is only as precise as the size of the tissue excised by LCM). While our results clearly indicate a large amount of silencing at P16, they also show that silencing does not warp the results from GFP-labeled neurons with barcodes. Silenced clones showed a similar spread within and across brain structures as GFP-labeled clones, and at least in aggregate they consistently did not reside as a single cluster. Notably, the average clone size was (despite few very large clones) very similar with and without silenced clones, indicating

that clones are preferentially silenced on an "all-or-nothing" basis, likely based on the position within the genome of retroviral insertion. Nonetheless, the quantification of silencing points out that our analysis at least with regard to the recovery of large clones systematically underestimates the number of lineally related neurons. As such, it will be important in the future to develop new retroviral vectors that are less prone to silencing.

Our findings seem to contradict two recent studies (Brown et al., 2011; Ciceri et al., 2013), which suggested that MGEderived clones form spatially isolated clusters in cortical columns or laminae. Both studies used low-titer retrovirus infections and defined clonality of post-migratory neurons based on geometric criteria. This unavoidably results in both lumping errors (clustered cells that are not clonal) and splitting errors (dispersed cells that are clonal but not recognized as such). While our results rule out that all members of a clone are preferentially clustered, we observed that subsets of clones in some instances reside in close proximity and form isolated clusters, consistent with the previous studies. As such, although clearly not an absolute rule, it remains possible that the members of a subset of clones have a spatial, and perhaps functional, relationship in the mature brain. Conversely, given that clonally related cells are produced in an environment that might expose them to similar guidance or other environmental cues, they may become clustered in a final location not due to lineage, but as a result of common environmental cues that guide their migration.

Work from a variety of organisms supports that lineage contributes to the generation of cell diversity. The role of lineage in invertebrate (Hobert, 2010) and vertebrate species has been both studied and compared (Cepko, 2014). In *Drosophila* and nematodes, it is very clear that specific lineages can generate predictable but highly divergent cell types (Hobert, 2010). In vertebrates, fewer studies have been carried out and lineage descriptions are much less comprehensive. However, clonal analysis in the retina has suggested that at least near terminal lineages may also be stereotyped (Godinho et al., 2007). However, whether these are derived from larger restricted lineages is not clear (Cepko, 2014).

Does the immense diversity of regionally specified cell populations within different brain circuits result from fate-restricted lineages? Given the vast expansion in neuronal numbers in the brain of mammals (Geschwind and Rakic, 2013; Molnár and Clowry, 2012), this is an attractive hypothesis. Our own efforts, as well as those of others, to examine the origins of interneurons within the forebrain demonstrate that specific progenitor zones, the MGE in particular (reviewed in Fishell and Rudy, 2011), give rise to the large majority of cortical and hippocampal interneuron populations. Similar work strongly suggests that subpallial structures, such as the striatum and amygdala derive their interneuron populations from the same embryonic sources (Marin et al., 2000; Nery et al., 2002). While certain commonalities exist, there are also marked differences in the abundance, intrinsic properties, and connectivity of interneurons within different telencephalic regions (Kawaguchi et al., 1995; Klausberger and Somogyi, 2008; Kubota and Kawaguchi, 1994).

These observations have prompted the question as to how such specificity is achieved and whether lineage restrictions play a role in this process. Several studies have demonstrated that the specification of interneuron subtypes is initiated during proliferative phases within the progenitor zones (Butt et al., 2008). However, region-specific migration of interneurons can still be altered during post-mitotic stages (e.g., McKinsey et al., 2013; van den Berghe et al., 2013). Thus, the expression of genes affecting the positioning of cells can potentially be dictated by lineage, as well as induced post-mitotically by environmental cues. For instance, recent work indicated that electrical activity influences the migration of post-mitotic interneurons (Bortone and Polleux, 2009; De Marco García et al., 2011), their morphological development, and their connectivity (Spiegel et al., 2014). Our results are consistent with environmental cues and stochastic choices affecting interneuron positioning independent of lineage.

Although not restricting sibling cells to specific structures, lineage may still contribute to the generation of interneuron diversity. For instance, one could imagine that specific lineages could create progeny that share a common program that is contextually modified after migration is completed. In such a model, the dispersion of a common pool of progenitors across structures could allow for different regions of the telencephalon to acquire interneurons with specific properties, while permitting them to adjust their functional program in accordance with the requirements of particular brain structures (Kepecs and Fishell, 2014). Furthermore, the MGE does not solely produce interneuron populations (Flandin et al., 2010; Nery et al., 2002). In vivo fate

mapping of the MGE has demonstrated that progenitor cells within this region give rise to GABAergic projection neurons of the globus pallidus (Flandin et al., 2010), as well as to portions of both the nucleus accumbens and amygdala (Nery et al., 2002). An important goal of future analysis will be to explore if there is a predictable lineage relationship between the diverse types of MGE-derived GABAergic populations.

In summary, our work demonstrates that individual MGE-derived lineages contribute to broad areas and distinct structures within the telencephalon. This indicates that regionally specific interneurons found in different brain circuits are not generated by dedicated progenitors within the MGE. However, whether an important role for lineage exists in the creation of specific interneuron populations and the underlying logic by which such lineages create diversity remains a possibility that is well worth exploring.

#### **EXPERIMENTAL PROCEDURES**

#### Mice and Ultrasound Backscatter Microscope-Assisted Injections

All mouse colonies were maintained in accordance with protocols approved by the IACUC at the NYU School of Medicine and IST Austria. The following mouse strains on a mixed background were used: Nkx2.1<sup>Cre/+</sup>;  $R26^{LSL-\bar{T}VAiLacZ/+}$  (Tg(Nkx2-1-cre)2Sand/J [Xu et al., 2008], R26TVAiLacZ [Seidler et al., 2008]) and Nestin-CreERT2;MADM-11 (Hippenmeyer et al., 2010). Embryos were staged in days post coitus, with embryonic day (E) 0.5 defined as noon of the day a vaginal plug was detected after overnight mating. In utero survival surgery and injection of retroviral vectors in the lateral ventricles of the embryonic mouse forebrains at E9.5-E12.5 was performed as previously described (Gaiano et al., 1999). Timed-pregnant dams were anesthetized with a sodium pentobarbital (0.6 mg/10 g body weight) solution containing magnesium sulfate (1.4 mg/10 g body weight [Mg<sub>2</sub>SO<sub>4</sub>, 7 H<sub>2</sub>O]). Surgical access to the uterine horns enabled the successive manipulation and placement of individual embryos under the UBM Probe using the ultrasound scanner Vevo 770 High-Resolution In Vivo Micro-Imaging System (FujiFilm VisualSonics) in order to visualize and guide the injection into embryonic ventricles. An oil-hydraulic manual microsyringe pump (MO-10, Narishige) was used to inject approximately 100 nl of the retroviral library (titer of ca. 108 cfu/ml) per embryo.

## **Sample Collection**

GFP-positive cells were collected individually using a laser microdissection system (LMD6000, Leica). Cells were collected into 20 μl of lysis buffer, including proteinase K (1:1,000; QIAGEN). Small patches of GFP-negative tissue next to the collected cell were frequently collected as a control.

## **Barcode Sequencing**

Cells were lysed and viral barcodes were PCR amplified from the viral vector via a two-step nested PCR. PCR conditions for the first PCR were 60°C annealing temperature with 35-s elongation time using 40 cycles. Primer sequences were SBR161-o1, gacaaccactacctgagcacccagt and SBR126-o2, ggctcgtactctataggcttcagctgtgga. PCR conditions for the nested PCR were 60°C annealing temperature with 35-s elongation time using 30 cycles. Primer sequences were SBR160-n1, atcacatggtcctgctggagttcgtga and SBR128-n2, attgttgagtcaaaactagagcctggacca. PCR products were visualized, gel purified (Gel Band Purification Kit, GE Healthcare), and sequenced.

### **Barcode Recovery from Silenced Vectors**

To recover barcodes from retrovirally infected cells that did not express GFP due to silencing, we collected large pieces of tissue from the same polyethylene terephthalate membrane slides using LCM. Tissues collected from different sections and different brain structures were processed separately to maintain spatial information of barcodes. Individual barcodes were sequenced from a large number of plasmids, each isolated from a single

bacterial colony. To estimate the number of barcodes per tissue, a minimum of six colonies were sequenced per sample. If more than one barcode was present, then up to 16 colonies were sequenced per sample. In a small number of instances (8 of 1,210 barcodes recovered in total), the same barcode was recovered in more than one brain and hemisphere. We assumed that this was the result of contamination or overrepresentation of that particular barcode in the retroviral library, and therefore any lineages marked by these eight barcodes were excluded from the analysis.

#### **MADM Clone Induction**

Embryonic MADM interval clones were generated as described previously (Hippenmeyer et al., 2010). Pregnant *MADM-11;Nestin-CreER*<sup>+/-</sup> females were injected intraperitoneally with a maximal dose of 2–3 mg tamoxifen (TM; dissolved in corn oil; Sigma) at E10. Embryos (*MADM-11*<sup>GT/TG</sup>;*Nestin-CreER*<sup>+/-</sup>) were isolated at E12 or E13, respectively, and brains were fixed in 4% paraformaldehyde (PFA)/PBS for 2–4 hr following cryopreservation in 30% sucrose/PBS. Cryosections 30-μm thick were obtained using a cryostat (Microm). The GFP and tdTomato signal was amplified by antibody staining, and nuclei were visualized using DAPI (Invitrogen). MADM clones in the MGE were imaged with a Zeiss LSM700 confocal microscope, and the total MADM clone size (#red + #green cells; average ± SEM) was determined for E10–E12 (n = 9) and E10–E13 (n = 8) clones, respectively. The efficiency of MADM clone induction was much lower in the ventral than in the dorsal telecephalon, and less than one MGE clone per brain was observed on average. In the absence of TM, no MADM labeling was observed.

#### **Data Analysis**

The average distance (i.e., the average distance between every pair of sibling neurons) and nearest-neighbor distance between sibling neurons was calculated after 3D reconstruction of the brain in Neurolucida software (MBF Bioscience). Cartesian coordinates of every barcode within the forebrain were exported from Neurolucida to MATLAB software (RRID: nlx\_153890; Mathworks), to calculate Euclidian distances between pairs of sibling neurons. A hierarchical, binary cluster tree was created by the linkage function and plotted into dendrograms. Data are presented as mean ± SD, and nonparametric tests (Mann-Whitney-Wilcoxon) were used for statistical significance estimations in Graphpad Prism software (RRID: rid\_000081).

### SUPPLEMENTAL INFORMATION

Supplemental Information includes Supplemental Experimental Procedures and five figures and can be found with this article online at http://dx.doi.org/10.1016/j.neuron.2015.07.011.

## **ACKNOWLEDGMENTS**

The authors are grateful to Robert Machold, Niels Ringstad, and Richard Tsien for their comments on the manuscript. Research in the G.F. laboratory is supported by NIH (NS 081297, MH095147, and P01NS074972) and the Simons Foundation. Research in the S.H. laboratory is supported by the European Union (FP7-CIG618444). C.M. is supported by EMBO ALTF (1295-2012). X.H.J. is supported by EMBO (ALTF 303-2010) and HFSP (LT000078/2011-L).

Received: March 24, 2015 Revised: May 29, 2015 Accepted: July 15, 2015 Published: August 20, 2015

#### **REFERENCES**

Bates, P., Young, J.A.T., and Varmus, H.E. (1993). A receptor for subgroup A Rous sarcoma virus is related to the low density lipoprotein receptor. Cell 74, 1032–1051

Bonaguidi, M.A., Wheeler, M.A., Shapiro, J.S., Stadel, R.P., Sun, G.J., Ming, G.-L., and Song, H. (2011). In vivo clonal analysis reveals self-renewing and multipotent adult neural stem cell characteristics. Cell *145*, 1142–1155.

Bortone, D., and Polleux, F. (2009). KCC2 expression promotes the termination of cortical interneuron migration in a voltage-sensitive calcium-dependent manner. Neuron *62*, 53–71.

Brown, K.N., Chen, S., Han, Z., Lu, C.-H., Tan, X., Zhang, X.-J., Ding, L., Lopez-Cruz, A., Saur, D., Anderson, S.A., et al. (2011). Clonal production and organization of inhibitory interneurons in the neocortex. Science *334*, 480–486

Bruno, R.M., Khatri, V., Land, P.W., and Simons, D.J. (2003). Thalamocortical angular tuning domains within individual barrels of rat somatosensory cortex. J. Neurosci. *23*, 9565–9574.

Butt, S.J.B., Sousa, V.H., Fuccillo, M.V., Hjerling-Leffler, J., Miyoshi, G., Kimura, S., and Fishell, G. (2008). The requirement of Nkx2-1 in the temporal specification of cortical interneuron subtypes. Neuron *59*, 722–732.

Cepko, C. (2014). Intrinsically different retinal progenitor cells produce specific types of progeny. Nat. Rev. Neurosci. 15, 615–627.

Cepko, C.L., Ryder, E., Austin, C., Golden, J., Fields-Berry, S., and Lin, J. (2000). Lineage analysis with retroviral vectors. Methods Enzymol. *327*, 118–145.

Ciceri, G., Dehorter, N., Sols, I., Huang, Z.J., Maravall, M., and Marín, O. (2013). Lineage-specific laminar organization of cortical GABAergic interneurons. Nat. Neurosci. *16*, 1199–1210.

Corbin, J.G., Nery, S., and Fishell, G. (2001). Telencephalic cells take a tangent: non-radial migration in the mammalian forebrain. Nat. Neurosci. 4 (Suppl), 1177–1182.

De Marco García, N.V., Karayannis, T., and Fishell, G. (2011). Neuronal activity is required for the development of specific cortical interneuron subtypes. Nature 472, 351–355.

Fishell, G., and Rudy, B. (2011). Mechanisms of inhibition within the telencephalon: "where the wild things are". Annu. Rev. Neurosci. 34, 535–567.

Flandin, P., Kimura, S., and Rubenstein, J.L.R. (2010). The progenitor zone of the ventral medial ganglionic eminence requires Nkx2-1 to generate most of the globus pallidus but few neocortical interneurons. J. Neurosci. *30*, 2812–2823.

Fuentealba, L.C., Rompani, S.B., Parraguez, J.I., Obernier, K., Romero, R., Cepko, C.L., and Alvarez-Buylla, A. (2015). Embryonic origin of postnatal neural stem cells. Cell *161*, 1644–1655.

Gaiano, N., Kohtz, J.D., Turnbull, D.H., and Fishell, G. (1999). A method for rapid gain-of-function studies in the mouse embryonic nervous system. Nat. Neurosci. 2, 812–819.

García-Moreno, F., Vasistha, N.A., Begbie, J., and Molnár, Z. (2014). CLoNe is a new method to target single progenitors and study their progeny in mouse and chick. Development *141*, 1589–1598.

Geschwind, D.H., and Rakic, P. (2013). Cortical evolution: judge the brain by its cover. Neuron *80*, 633–647.

Godinho, L., Williams, P.R., Claassen, Y., Provost, E., Leach, S.D., Kamermans, M., and Wong, R.O.L. (2007). Nonapical symmetric divisions underlie horizontal cell layer formation in the developing retina in vivo. Neuron *56*, 597–603.

Golden, J.A., Fields-Berry, S.C., and Cepko, C.L. (1995). Construction and characterization of a highly complex retroviral library for lineage analysis. Proc. Natl. Acad. Sci. USA *92*, 5704–5708.

Halliday, A.L., and Cepko, C.L. (1992). Generation and migration of cells in the developing striatum. Neuron 9, 15–26.

Hippenmeyer, S., Youn, Y.H., Moon, H.M., Miyamichi, K., Zong, H., Wynshaw-Boris, A., and Luo, L. (2010). Genetic mosaic dissection of Lis1 and Ndel1 in neuronal migration. Neuron *68*, 695–709.

Hobert, O. (2010). Neurogenesis in the nematode Caenorhabditis elegans. WormBook  $Oct\ 4$ , 1–24.

Kawaguchi, Y., Wilson, C.J., Augood, S.J., and Emson, P.C. (1995). Striatal interneurones: chemical, physiological and morphological characterization. Trends Neurosci. 18, 527–535.

Kepecs, A., and Fishell, G. (2014). Interneuron cell types are fit to function. Nature 505, 318-326.

Kessaris, N., Fogarty, M., Iannarelli, P., Grist, M., Wegner, M., and Richardson, W.D. (2006). Competing waves of oligodendrocytes in the forebrain and postnatal elimination of an embryonic lineage. Nat. Neurosci. 9, 173-179.

Klausberger, T., and Somogyi, P. (2008). Neuronal diversity and temporal dynamics: the unity of hippocampal circuit operations. Science 321, 53-57.

Kohwi, M., and Doe, C.Q. (2013). Temporal fate specification and neural progenitor competence during development. Nat. Rev. Neurosci. 14, 823-838.

Kubota, Y., and Kawaguchi, Y. (1994). Three classes of GABAergic interneurons in neocortex and neostriatum. Jpn. J. Physiol. 44 (Suppl 2), S145-S148.

Marin, O., Anderson, S.A., and Rubenstein, J.L. (2000). Origin and molecular specification of striatal interneurons. J. Neurosci. 20, 6063-6076.

McCarthy, M., Turnbull, D.H., Walsh, C.A., and Fishell, G. (2001). Telencephalic neural progenitors appear to be restricted to regional and glial fates before the onset of neurogenesis. J. Neurosci. 21, 6772-6781.

McKinsey, G.L., Lindtner, S., Trzcinski, B., Visel, A., Pennacchio, L.A., Huylebroeck, D., Higashi, Y., and Rubenstein, J.L.R. (2013). Dlx1&2-dependent expression of Zfhx1b (Sip1, Zeb2) regulates the fate switch between cortical and striatal interneurons. Neuron 77, 83-98.

Miyoshi, G., Butt, S.J.B., Takebayashi, H., and Fishell, G. (2007). Physiologically distinct temporal cohorts of cortical interneurons arise from telencephalic Olig2-expressing precursors. J. Neurosci. 27, 7786-7798.

Molnár, Z., and Clowry, G. (2012). Cerebral cortical development in rodents and primates. Prog. Brain Res. 195, 45-70.

Mountcastle, V.B. (2003). Introduction. Computation in cortical columns. Cereb. Cortex 13, 2-4.

Nery, S., Fishell, G., and Corbin, J.G. (2002). The caudal ganglionic eminence is a source of distinct cortical and subcortical cell populations. Nat. Neurosci. 5. 1279-1287.

Noctor, S.C., Flint, A.C., Weissman, T.A., Dammerman, R.S., and Kriegstein, A.R. (2001). Neurons derived from radial glial cells establish radial units in neocortex. Nature 409, 714-720.

Noctor, S.C., Martínez-Cerdeño, V., Ivic, L., and Kriegstein, A.R. (2004). Cortical neurons arise in symmetric and asymmetric division zones and migrate through specific phases. Nat. Neurosci. 7, 136-144.

Rakic, P. (1988). Specification of cerebral cortical areas. Science 241, 170\_176

Seidler, B., Schmidt, A., Mayr, U., Nakhai, H., Schmid, R.M., Schneider, G., and Saur, D. (2008). A Cre-loxP-based mouse model for conditional somatic gene expression and knockdown in vivo by using avian retroviral vectors. Proc. Natl. Acad. Sci. USA 105, 10137-10142.

Southwell, D.G., Paredes, M.F., Galvao, R.P., Jones, D.L., Froemke, R.C., Sebe, J.Y., Alfaro-Cervello, C., Tang, Y., Garcia-Verdugo, J.M., Rubenstein, J.L., et al. (2012). Intrinsically determined cell death of developing cortical interneurons, Nature 491, 109-113.

Spiegel, I., Mardinly, A.R., Gabel, H.W., Bazinet, J.E., Couch, C.H., Tzeng, C.P., Harmin, D.A., and Greenberg, M.E. (2014). Npas4 regulates excitatoryinhibitory balance within neural circuits through cell-type-specific gene programs. Cell 157, 1216-1229.

Tricoire, L., Pelkey, K.A., Erkkila, B.E., Jeffries, B.W., Yuan, X., and McBain, C.J. (2011). A blueprint for the spatiotemporal origins of mouse hippocampal interneuron diversity. J. Neurosci. 31, 10948-10970.

van den Berghe, V., Stappers, E., Vandesande, B., Dimidschstein, J., Kroes, R., Francis, A., Conidi, A., Lesage, F., Dries, R., Cazzola, S., et al. (2013). Directed migration of cortical interneurons depends on the cell-autonomous action of Sip1. Neuron 77, 70-82.

Vasistha, N.A., García-Moreno, F., Arora, S., Cheung, A.F.P., Arnold, S.J., Robertson, E.J., and Molnár, Z. (2014). Cortical and clonal contribution of Tbr2 expressing progenitors in the developing mouse brain. Cereb. Cortex Jun 13. bhu125.

Walsh, C., and Cepko, C.L. (1992). Widespread dispersion of neuronal clones across functional regions of the cerebral cortex. Science 255, 434-440.

Xu, Q., Tam, M., and Anderson, S.A. (2008). Fate mapping Nkx2.1-lineage cells in the mouse telencephalon. J. Comp. Neurol. 506, 16-29.

Yu, Y.-C., Bultje, R.S., Wang, X., and Shi, S.-H. (2009). Specific synapses develop preferentially among sister excitatory neurons in the neocortex. Nature 458, 501-504.

Zong, H., Espinosa, J.S., Su, H.H., Muzumdar, M.D., and Luo, L. (2005). Mosaic analysis with double markers in mice. Cell 121, 479-492.